Sensitivity of Moist Convection Forced by Boundary Layer Processes to Low-Level Thermodynamic Fields

N. ANDREW CROOK

National Center for Atmospheric Research, Boulder, Colorado*

(Manuscript received 21 August 1995, in final form 18 January 1996)

ABSTRACT

The sensitivity of moist convection to a number of low-level thermodynamic parameters is examined with a high-resolution, nonhydrostatic numerical model. The parameters examined are the surface temperature dropoff (defined as the difference between the potential temperature measured at the surface and that in the well-mixed boundary layer), the surface moisture dropoff (defined similarly for moisture), the boundary layer moisture dropoff (defined as the vertical decrease in moisture within the boundary layer), and the depth of the moisture. The typical variability in these parameters is estimated from two field experiments in northeastern Colorado. Sensitivity is then defined relative to this typical observational variability.

Two convection initiation cases from northeastern Colorado are examined. In both cases, convection initiation is found to be most sensitive to the surface temperature dropoff and the surface moisture dropoff. It is found that variations in boundary layer temperature and moisture that are within typical observational variability (1°C and 1 g kg^{-1}, respectively) can make the difference between no initiation and intense convection. For cases in which convection is well developed, the storm's strength is more sensitive to the typical observational variability in moisture than in temperature. However, at the convection/no convection boundary, the storm's strength is more sensitive to the surface temperature dropoff than to the surface moisture dropoff (both in terms of equivalent moist static energy and, for the cases studied, in terms of typical observational variability). It is shown that this is due to the greater sensitivity of the negative area (or convective inhibition) to temperature variations than to moisture variations. The implications of these results for the predictability of convection initiation are then briefly discussed.

1. Introduction

Accurately predicting the development of severe thunderstorms is one of the most challenging problems facing weather forecasters. Currently, forecasters rely on a number of different data sources to aid them in these predictions. These sources include the National Weather Service soundings, surface stations, satellites, radars and lightning detection networks. In recent years there has been a considerable effort to combine these separate data sources into gridded analysis and short-term prediction systems. These systems include the Mesoscale Analysis and Prediction System (MAPS, Benjamin 1989) the Local Analysis and Prediction System (LAPS, McGinley 1989), as well as a number of variants on LAPS such as Oklahoma-LAPS (O-LAPS, Brewster et al. 1994) and Terminal-LAPS (T-LAPS, Cole et al. 1993).

The analysis cycles of these systems should provide guidance to the human forecaster in short-term thunderstorm prediction. However, it is still an open question as to whether the predictive cycle of these systems will be able to produce accurate, *explicit,* thunderstorm forecasts. The purpose of this study is to explore the prospects for explicit thunderstorm prediction by examining the sensitivity of convection initiation to a number of boundary layer thermodynamic parameters. The approach taken is sometimes called the "forward" method, where a forward simulation is performed from an initial state and then compared with simulations from slightly perturbed initial states. Examples of studies utilizing this approach are Weisman and Klemp (1982), Droegemeier and Wilhelmson (1985a) and (1985b), and Lee et al. (1991). Clearly, this is a somewhat limited approach since to calculate the sensitivity to each perturbation around each initial state requires a separate, forward, integration.

Recently, the adjoint method has proven to be a powerful tool for examining the sensitivity of atmospheric flows (see, e.g., Errico and Vukicevic 1992). With this method, it is possible to examine the sensitivity of some measure (e.g., the strength of an updraft) to the initial fields with a single integration of the forward model and one of the adjoint. However, adjoint models are

* The National Center for Atmospheric Research is sponsored by the National Science Foundation.

Corresponding author address: Dr. N. Andrew Crook, NCAR/MMM, P.O. Box 3000, Boulder, CO 80307-3000.

usually complex to code and, to the author's knowledge, the only adjoint of a cloud model that presently exists is that described in Sun et al. (1994). Furthermore, the sensitivity calculated by the adjoint method is limited to linear variations of the measure, and thus would be of less utility in the convection initiation cases examined in this study.

Before the results from either method (forward or adjoint) can be applied to a specific atmospheric event, it is necessary to make a number of assumptions about the model and the control simulation. The first assumption that is made in this study is that the sensitivity of the model reflects the real atmosphere's sensitivity. The second assumption is that the control experiment accurately simulates the atmospheric event being examined. Obtaining an accurate simulation (i.e., one that minimizes the model/data discrepancy) is the problem of four-dimensional data assimilation. If an adjoint of the forward model exists then the model/data discrepancy can be systematically reduced by using the method of steepest descent. If an adjoint does not exist then this model/data discrepancy can be reduced only through trial and error. In this work, a further assumption is made that even if an accurate simulation has not been produced, the sensitivity of this "less-than-optimal" simulation reflects the sensitivity of an optimal experiment.

In the present study the forward method is used to examine the sensitivity of two convective cases observed in northeastern Colorado to thermodynamic properties of the boundary layer. The technique described in Crook (1994) and Crook and Tuttle (1994) is used to initialize a small-scale model with radar, surface, and sounding data. The assumption is made that the dynamic fields have been accurately represented in the initial conditions and then the thermodynamic properties of the boundary layer are varied.

The outline of the paper is as follows. In section 2, the initialization method is described and then some of the sources of error in the thermodynamic field are examined. In section 3, the methodology of the sensitivity studies is discussed. In section 4, two case studies are described and then the sensitivity to some of the thermodynamic errors identified in section 2 is examined. Section 5 contains an analysis of the results found in the sensitivity experiments, and in section 6 the implications of these results are discussed. Finally, conclusions are given in section 7.

2. Initialization method

The technique for initializing the numerical model has been described in detail in two recent papers, Crook (1994) and Crook and Tuttle (1994). Here this technique is briefly reviewed.

a. Velocity fields

The initialization commences by interpolating the wind observations to the model grid. These observations are derived from Doppler radar, a surface mesonet, and a single upper-air sounding as shown schematically in Fig. 1. To estimate the horizontal wind component transverse to the radar beam, a technique called TREC [tracking radar echoes by correlation, Tuttle and Foote (1990)] is used. TREC estimates the horizontal wind by tracking small reflectivity features in the boundary layer using a cross-correlation method. Typically, the radar-derived data extends up to 2–3 km AGL in the High Plains. A standard Cressman filter is used to interpolate the velocity data to the model grid.

b. Temperature fields

The thermodynamic retrieval method of Gal-Chen (1978) is used to derive the pressure and temperature perturbations in the boundary layer. The acceleration terms are calculated by fitting a least squares curve to the velocity data over a number of time levels. In the traditional retrieval technique, the pressure and temperature are accurate only to a horizontal constant, which is usually obtained from a nearby sounding. However, in many cases, the nearest sounding may not be representative of the area of interest. As will be seen, this can have an important effect on the model's ability to forecast convection.

One method for obtaining a more representative sounding, which is often used by operational forecasters, is to adjust an earlier sounding based on current surface observations. This is generally done by assuming a well-mixed boundary layer with a potential temperature equal to the current observed surface value. However, mixing out the boundary layer based on the surface temperature will generally introduce error into the initial fields. In a recent paper by Mueller et al. (1993), the boundary layer potential temperatures from 290 Cross-chain Loran Atmospheric Sounding System (CLASS) launches were compared with nearby surface mesonet stations (either collocated or within 5 km) from the Convection Initiation and Downburst Experiment (CINDE). The statistics of this intercomparison are listed in Table 1. The standard deviation between

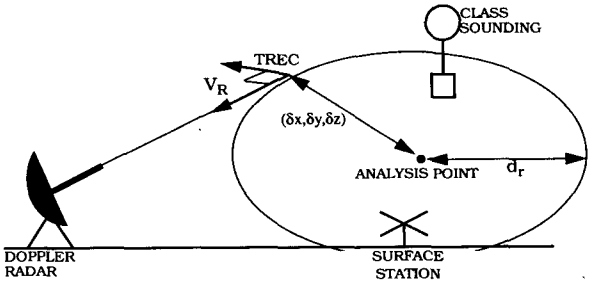

FIG. 1. Schematic showing the data sources that are used in the model initialization. Here, d_r is the radius of influence of the Cressman filter and $(\delta x, \delta y, \delta z)$ is the vector displacement from the model grid point to the data location.

the two measurements was 2.1°C. Only a small bias of 0.2°C was found between the surface and sonde measured potential temperature, with the sonde measurement being warmer. This intercomparison has been repeated with data collected during the Realtime Analysis and Prediction of Storms (RAPS) experiment conducted in northeastern Colorado in 1992 and 93, Neilley et al. (1993). This dataset includes observations from PROFS (Program for Regional Observing and Forecasting Systems) mesonet stations. The intercomparison has also been limited to cases where the sounding was collocated with the mesonet station. This intercomparison produced a standard deviation of 0.7°C and a surface warm bias of 1.0°C.

Possible reasons for the difference between the potential temperature measured by a surface station and that measured by a sonde in the boundary layer include instrument error and error of representativeness. Temperatures measured by the mesonet stations and CLASS sondes have an rms accuracy of about 0.5°C (C. Wade, personal communication). Also the sensors used in the mesonet stations and CLASS sondes are not the same and may have different instrument responses. The second possible reason is that the mesonet station is sensing air in the surface layer, which is often superadiabatic during the day. In a heated boundary layer, the surface potential temperature should be greater than the sonde-measured value and probably accounts for the 1.0°C bias found from the RAPS experiment. The reason that the warm bias in the CINDE dataset is significantly less is not known at present.

c. *Moisture fields*

The initialization of the water vapor field presents even more difficulties than that of the temperature field, since moisture data are usually only available from surface stations and widely separated soundings. To initialize the water vapor field from these data sources it is necessary to make a number of assumptions about the vertical distribution of moisture throughout the boundary layer. To investigate this distribution, 125 soundings from the RAPS experiment were examined. The moisture profile for each sounding was normalized by the mixing ratio measured by the sounding in the lowest 200 m of the atmosphere q_{surf}, and by the depth of the boundary layer.[1] The mean normalized profile and standard deviation are plotted in Fig. 2. On the average, the moisture decreases monotonically from its value near the surface to $0.85q_{surf}$ at the top of the boundary layer. The standard deviation increases monotonically to $0.15q_{surf}$ at the top of the boundary layer.

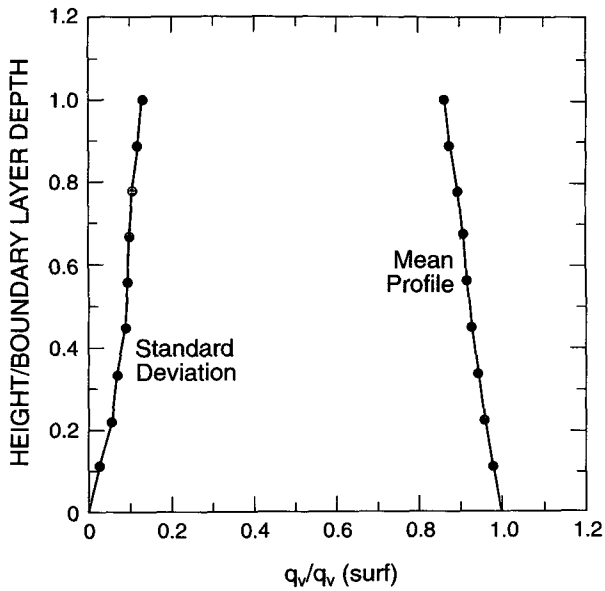

FIG. 2. Mean and standard deviation profile of moisture throughout the boundary layer from 125 soundings from the RAPS experiment.

The profile shown in Fig. 2 was normalized by the near-surface moisture measured by a sonde. Another source of variability results from the fact that this value in general will differ from the moisture measured by a surface station. This difference was investigated by Mueller et al. (1993), who found that from 290 soundings, the mesonet mixing ratios averaged 1.0 g kg^{-1} greater than the mixing ratios measured by the soundings over the lowest 50 mb of the atmosphere. The standard deviation of the difference was 1.1 g kg^{-1}. This difference has also been investigated with data from the RAPS experiment. In this dataset the surface mesonet value averages 0.7 g kg^{-1} more moist than the mean value measured by the sounding over the lowest

TABLE 1. Typical errors in thermodynamic parameters ($\Delta\theta_{surf}$ in degrees C, Δq_{surf} in grams per kilogram).

Experiment		Standard deviation	Bias
CINDE	$\Delta\theta_{surf}$	2.1	0.2
	Δq_{surf}	1.0	1.1
RAPS	$\Delta\theta_{surf}$	0.7	1.0
	Δq_{surf}	0.9	0.7
	Δq_{bdy}	0.15	0.15
Sensitivity experiments	$\Delta\theta_{surf}$	1.0	1.0
	Δq_{surf}	1.0	1.0
	Δq_{bdy}	0.15	−0.15
	Δh_{bdy}	0.25	0.0

[1] Since our purpose is to obtain an estimate of the moisture at the lowest level of the boundary layer and as there is some variation in moisture across the boundary layer, q_{surf} has been calculated over a shallower depth (200 m) than potential temperature, which tends to be more well mixed.

200 m of the atmosphere. The standard deviation of the difference was 0.9 g kg^{-1}.

Mahrt (1976) has also examined the average moisture profile in the High Plains convective boundary layer from soundings taken during the National Hail Research Experiment (NHRE). His analysis was restricted to midafternoon (1400 local time) soundings taken on relatively cloud-free days. Figure 2 of Mahrt (1976) indicates that, on the average, the moisture decreases approximately linearly to a value at the top of the boundary layer of 60% of the surface value. However, this decrease includes the decrease between the surface-measured value and the value at the top of the surface layer, which has not been included in our Fig. 2. The decrease across the boundary layer (excluding the surface layer) is approximately 30% in Mahrt's analysis. This is a somewhat larger decrease than found from the RAPS soundings (15%). One reason for this difference may be that the present analysis has included a number of soundings taken earlier in the day (1100 local time) when there is generally a larger cap at the top of the boundary layer. Under these circumstances, the moisture is usually distributed more evenly throughout the boundary layer.

3. Methodology of sensitivity experiments

The base state sounding that is used in the sensitivity experiments is shown schematically in Fig. 3. Throughout the boundary layer, it is assumed that the potential temperature is constant while the mixing ratio decreases linearly. With these assumptions, the sounding is controlled by three parameters. These are

1) $\Delta\theta_{surf}$, the surface potential temperature dropoff. The difference between the surface measured potential temperature and the boundary layer value;

2) Δq_{surf}, the surface moisture dropoff. The difference between the mixing ratio measured at the surface and the value in the lowest levels of the boundary layer;

3) Δq_{bdy}, the boundary layer moisture dropoff. The fractional decrease in the mixing ratio from the bottom to the top of the boundary layer.

The sensitivity to a fourth parameter, Δh_{bdy}, which is the ratio of the depth of the linear moisture profile to the depth of the boundary layer, is also examined. Although the mean moisture profile in Fig. 2 showed a linear variation throughout the depth of the boundary layer, often a distinct two-layer structure exists in individual soundings. In these cases, the moisture is relatively constant through a certain depth of the boundary layer and then has a rapid dropoff to a second value. In Mueller et al. (1993), it was found that convection can be very sensitive to moisture profiles with this structure.

The values used for the four parameters in the control experiment are listed in Table 1. Also listed are the

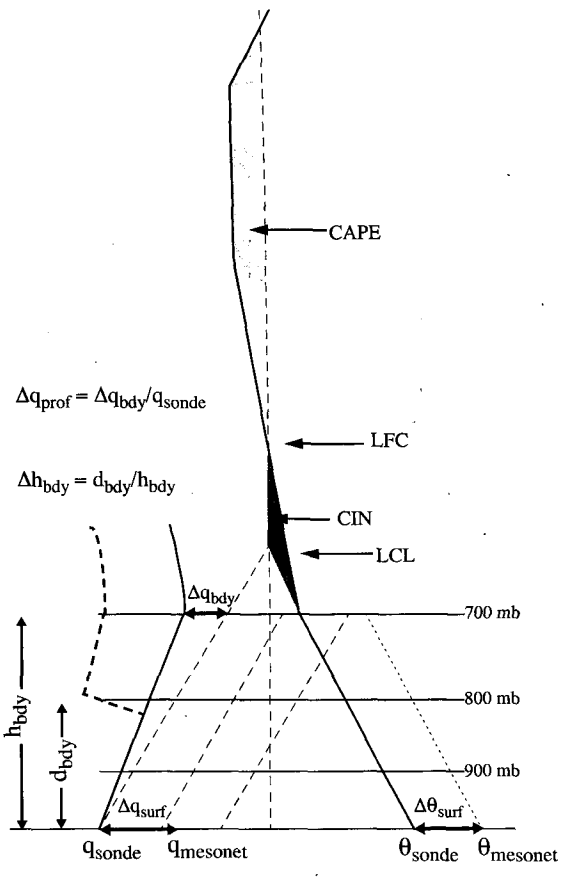

FIG. 3. Schematic of base-state sounding showing the four control parameters, $\Delta\theta_{surf}$, Δq_{surf}, Δq_{bdy}, and Δh_{bdy}, which are varied in the sensitivity experiments. The dashed mixing ratio line illustrates how the moisture profile changes as the parameter Δh_{bdy} is varied. The relative decrease in moisture at the height, d_{bdy}, is set at 50%.

values observed from the CINDE and RAPS experiment. As already noted, there is some difference in the bias and standard deviation of $\Delta\theta_{surf}$ observed in the CINDE and the RAPS experiment. For the sensitivity experiments, values similar to those observed during the RAPS experiment (bias = 1.0°C, σ = 1.0°C.) are taken since the cases occurred during this field experiment. The bias and standard deviation for Δq_{surf} are both set to 1.0 g kg^{-1}, which is similar to the values observed during both CINDE and RAPS. For Δq_{bdy} the bias is -0.15 and $\sigma = 0.15$ (similar to the values observed during RAPS). In the sensitivity experiments, Δq_{bdy} is not increased greater than one standard deviation (which is the case of a well-mixed moisture profile) since it is extremely rare to find convective boundary layers in which the mixing ratio increases upward. Finally, $\Delta h_{bdy} = 1$ is taken for the control; that is, the depth of the moisture is the same as the depth of the boundary layer.

Two measures will be used to determine the strength of convection. Both measures are the maximum value that occur during the simulation period of 2 h:

(a) Σq_r, the integral of the rain water field over the total domain;

(b) w_{max}, the maximum vertical velocity in the domain.

In this study the sensitivity of these measures to the four parameters discussed above will be compared. To facilitate this comparison, the variations of these parameters will be normalized by the standard deviations listed in Table 1. Accordingly, if it is found that Σq_r varies more as parameter A is changed by one standard deviation compared to varying parameter B, then it will be stated that Σq_r is more sensitive to parameter A than B.

The model used in this study is the anelastic, nonhydrostatic model described in Clark (1977) and Clark and Farley (1984). The model equations are cast in a nonorthogonal, terrain-following system of coordinates. The subgrid-scale turbulent processes are parameterized using the first-order closure of Lilly (1962) and Smagorinsky (1963) (Clark and Farley 1984). Only warm-rain processes [which follow the parameterization of Kessler (1969)] are considered in this study. In the majority of simulations, $\Delta x = \Delta y = 2.5$ km, $\Delta z = 300$ m, and the size of the model domain is 125 km $\times$ 125 km $\times$ 16 km. A time step $\Delta t = 10$ s is used.

4. Case studies

a. 21 June 1993

On this day, a line of intense convection developed just to the east of Denver around 1400 LT (all times listed in local time, which is UTC minus 6 h). The convection developed along a low-level convergence line that formed very rapidly between 1300 and 1400 LT. This convergence line developed as a cold air surge, forced by previous convection over the Rocky Mountains, propagated eastward, and encountered the low-level southeasterlies over the Plains. The cold air surge continued to propagate eastward at a speed of approximately 8 m s^{-1} as convection developed along and slightly behind the convergence line. The reflectivity from Mile High Radar (MHR) at an elevation of 1.2° at 1440 LT is shown in Fig. 4. The convergence line at this time is approximately 30 km to the east of Mile High Radar. About 10 km to the west of the convergence line, several 60-dBZ storms have developed.

The sounding used in the control experiment is shown in Fig. 5 and is based on a CLASS sounding taken at Stapleton International Airport at 1100 LT. The CLASS sounding has been modified by mixing out the boundary layer based on a surface temperature of 29°C. This value was obtained by subtracting the mean surface temperature bias of 1.0°C (see Table 1) from the temperature observed at Stapleton at 1300 LT, which was 30°C.

The control experiment was initialized at 1300 LT and integrated for 2 h. A horizontal cross section of the predicted rainwater and velocity field at 1400 LT is shown in Fig. 6a. A line of storms has developed in the simulation, which are within 5 km of the observed location. Figure 6b is an east–west cross section of the rainwater field along the line AA' shown in 6a. The maximum in rainwater occurs just west of the low-level convergence line at an altitude of 7.5 km AGL. Rain is falling out to the west of the convergence line and reaches the surface 10 min after the time shown in Fig. 6. The integrated rainwater field, Σq_r, maximizes at a value of 2.03×10^8 kg. (Since this magnitude does not have much meaning per se, the rainwater masses in the other experiments are normalized by this value.) The maximum vertical velocity $w_{max} = 24.8$ m s^{-1}. A time series of the integrated rainwater from the control experiment is plotted in Fig. 7.

To examine the effect of model resolution, the control experiment was repeated with the horizontal grid-length reduced to 1.5 km. The time series of Σq_r from this simulation is also plotted in Fig. 7, and shows a similar trend to the control with an increase in the maximum rainwater of 25%. The vertical velocity also exhibited a similar trend with the maximum being 30% greater than the control.

To verify the model results, Σq_r was compared with the integrated rainwater estimated from the observed radar reflectivity. Estimating rainwater from reflectivity has been the subject of numerous studies [see Battan (1973) for an extensive list]. It is well recognized that these estimates are generally only accurate to a factor of 2 or 3. Consequently, two Z–M relationships have been used, one which gives an estimate on the high side of the relationships in Battan (1973) and one on the low side, to indicate the range of likely rainwater totals. The first relationship, from Jones (1956) is

$$Z = 3.0 \times 10^4 M^{1.41}, \tag{4.1}$$

where M is expressed in grams per cubic meter. The second relationship from Morgan and Mueller (1972) is

$$Z = 2.0 \times 10^4 M^{1.67}. \tag{4.2}$$

The integrated rainwater calculated from the two relationships is plotted in Fig. 7. As can be seen, the modeled convection in both the control and the higher-resolution simulation develops at about the same time as the observed case, and have maximum values which fall between the maxima calculated by the two Z–M relationships. However, some differences in the rate of growth are apparent. First, the modeled rainwater develops faster than the rainwater calculated by both Z–M relationships. Second, the modeled rainwater decreases after reaching a maximum at 1430 LT, whereas the observed rainwater continues to increase after 1430 LT.

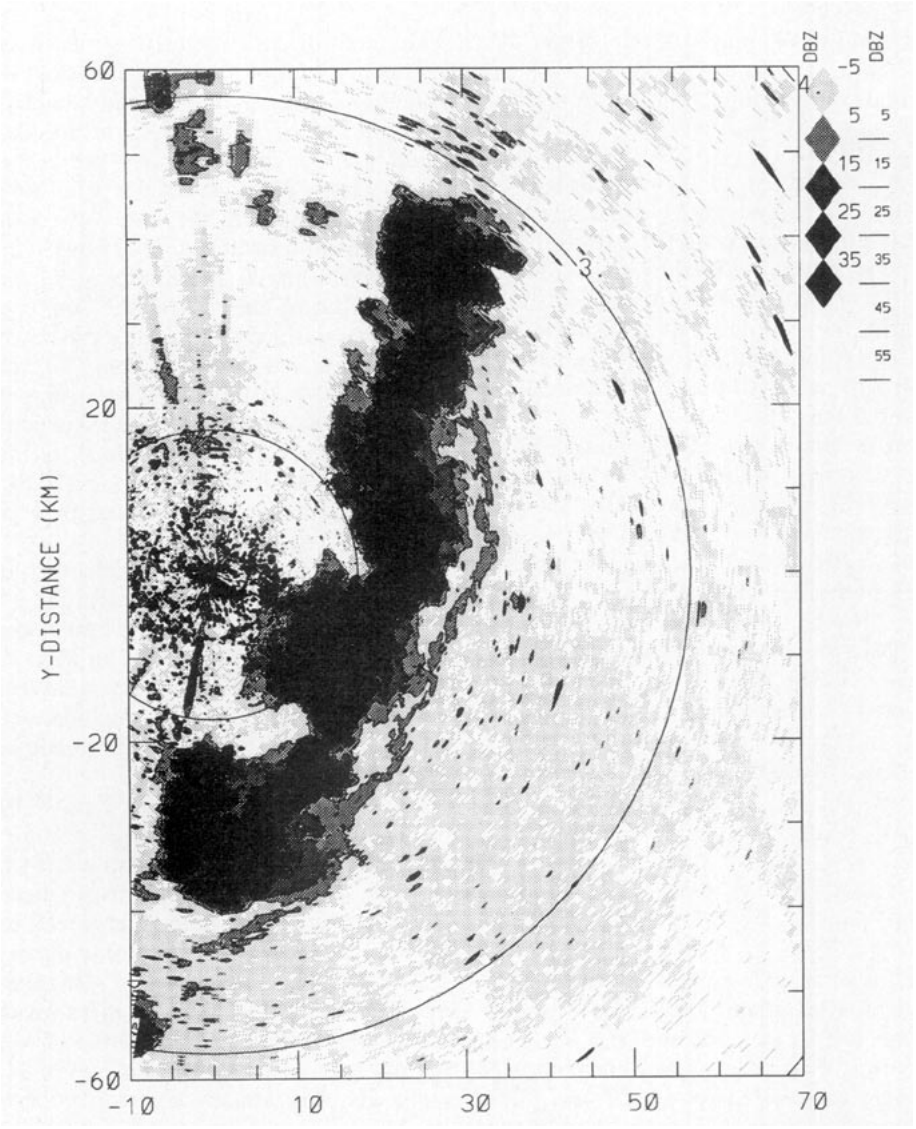

FIG. 4. Reflectivity at an elevation of 1.2° measured by Mile High Radar at 1440 LT June 21. All reflectivity above 25 dBZ is shown as solid black. The maximum reflectivity at this time is approximately 65 dBZ. Note the convergence line just to the east of the line of storms.

Despite these differences it is felt that the model has simulated the initial storm evolution, which is the focus of this study, with reasonable accuracy. As discussed in the introduction, in this study the assumption has been made that the sensitivity of this simulated storm reflects the sensitivity of a simulation in which the model/data discrepancy has been minimized (as could be done with the adjoint technique).

The sensitivity of the total rainwater and the maximum vertical velocity to the four boundary layer parameters is now examined. Figure 8 shows the variation of Σq_r and w_{max} against (i) $\Delta\theta_{surf}$, (ii) Δq_{surf}, (iii) Δq_{bdy}, and (iv) Δh_{bdy}.

As can be seen from Fig. 8a, the total rainwater produced, Σq_r, is most sensitive to $\Delta\theta_{surf}$. At one standard deviation less than the control, no convection develops. At one standard deviation greater than the control, Σq_r increases by a factor of 3.9, at 2σ by a factor of 4.75.

The maximum vertical velocity w_{max} also shows a strong sensitivity to $\Delta\theta_{surf}$, particularly for values less than the control. At $\Delta\theta_{surf} = -1\sigma$, w_{max} decreases to 3.0 m s^{-1} (this maximum velocity occurs in the convergence line, since no convection develops in this simulation). For positive values of $\Delta\theta_{surf}$, w_{max} increases only slowly. This is a feature that occurs in both case studies and will be discussed in more detail in section 5.

The total rainwater also shows a strong sensitivity to the surface moisture dropoff. At $\Delta q_{surf} = -2\sigma$, no convection develops, at -1σ, $\Sigma q_r = 0.27$, at $+1\sigma$, Σq_r

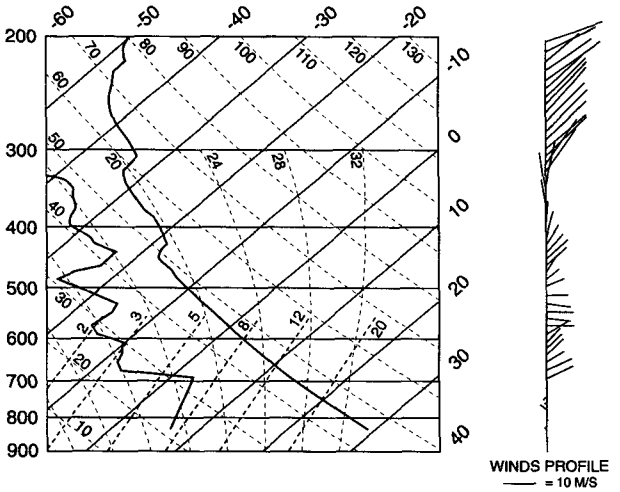

FIG. 5. Sounding used to initialize the 21 June control simulation. Sounding is the same as the CLASS sounding taken at 1100 LT except that the boundary layer has been mixed out based on a surface temperature of 29°C. The wind vectors on the right point in the direction of the wind.

= 2.3 greater and at $+2\sigma$, $\Sigma q_r = 3.7$. The maximum vertical velocity varies from 5.0 m s^{-1} at -2σ to 33.0 m s^{-1} at $+2\sigma$. Note that when convection develops, w_{max} is more sensitive to moisture variations than to temperature variations. Again, this is a feature that occurs in both case studies and will be discussed in section 5.

The sensitivity of the convection to Δq_{bdy} and Δh_{bdy} is significantly less than for the other two parameters. As Δq_{bdy} varies from -2σ to $+\sigma$, Σq_r increases from 0.4 to 1.49, while the maximum vertical velocity increases from 22.4 to 26.9 m s^{-1}. As Δh_{bdy} varies from 0.25 to 1.0, Σq_r changes from 0.35 to 1.0, while w_{max} increases from 22.3 to 24.8 m s^{-1}.

Simulations with varying $\Delta\theta_{surf}$ and Δq_{surf} were also performed at higher resolution ($\Delta x = 1.5$ km). The two measures, Σq_r and w_{max}, showed a similar sensitivity to $\Delta\theta_{surf}$ and Δq_{surf} in these higher-resolution simulations. Specifically, convection was shut off at both $\Delta\theta_{surf} = -\sigma$ and $\Delta q_{surf} = -2\sigma$.

To illustrate the reason for the strong sensitivity to the surface temperature dropoff, $\Delta\theta_{surf}$, vertical cross sections are plotted along the line AA' from the control simulation and the simulation with the boundary layer cooled by one standard deviation (1°C). Figure 9a shows the velocity field and the perturbation potential temperature field θ' from the control simulation after 50 min of integration. Figure 9b shows the same fields from $\Delta\theta_{surf} = -1\sigma$ simulation. (The θ' field represents the perturbation from that experiment's base state sounding, which varies between the two experiments.) The first point to note about Figs. 9a and 9b is that the boundary layer is deeper in the control experiment since it has been mixed out to a greater depth. The second point is that negative buoyancy has developed near the top of the convergence line in the region where the updraft pushes into the stratified layer above the boundary layer. (Since no cloud water has formed at this time, it can be assumed that latent heating has not affected the temperature field.) This negative buoyancy causes the air in the updraft to decelerate above the boundary layer. In both experiments, the updraft extends to approximately 900 m above the top of the boundary layer. However, since the boundary layer is deeper in the control experiment, the updraft reaches a greater height and is able to lift air to the level of free convection (LFC). In other words, the energy needed to lift air to the LFC, the negative area, is less in the control experiment. Based on a surface mixing ratio of 8 g kg^{-1}, the negative area in the control simulation is 20 J kg^{-1}, while in the -1σ simulation the negative area is 60 J kg^{-1} (an increase of a factor of 3).

Although the primary concern of this study is the sensitivity to low-level thermodynamics, one simulation with varying dynamics is presented to illustrate the complexity of the convection initiation problem. Figure 9b indicates that the updraft is being sheared off to the east by the westerlies above the boundary layer. To examine the influence of these westerlies, the simulation shown in Fig. 9b was repeated with the winds above the boundary layer set to zero. As shown in Fig. 9c, the updraft in this simulation is stronger and able to penetrate further into the stable layer. Convection now forms in this simulation with a strength similar to that found in the control experiment. These experiments indicate that convection initiation is very sensitive to both the stability and the shear at the top of the boundary layer. A similar sensitivity to shear was found by Weisman and Klemp (1982) in their simulations of storms generated by low-level warm perturbations. It is planned to investigate the sensitivity to shear above the boundary layer in a future study.

The 21 June case has shown a strong sensitivity to variations in the initial thermodynamic fields, particularly the surface temperature and moisture dropoff, which are within the accuracy of the present observing system. A second case from RAPS93 is now examined in order to explore how general this result is.

b. 15 July 1993

On this day, a stationary east–west convergence line formed over Denver and persisted for several hours. A CLASS sounding taken at 1400 LT, 20 km to the east of Mile High Radar and 5 km south of the convergence line, is shown in Fig. 10. The potential temperature profile is well mixed up to 2200 m AGL and then has a fairly uniform stratification of 3°C km^{-1} up to 7 km. At 7 km, an inversion of 3°C exists.

Around 1550 LT, several convective storms developed as a low-level wind surge moved up from the south and strengthened the convergence line. Reflectiv-

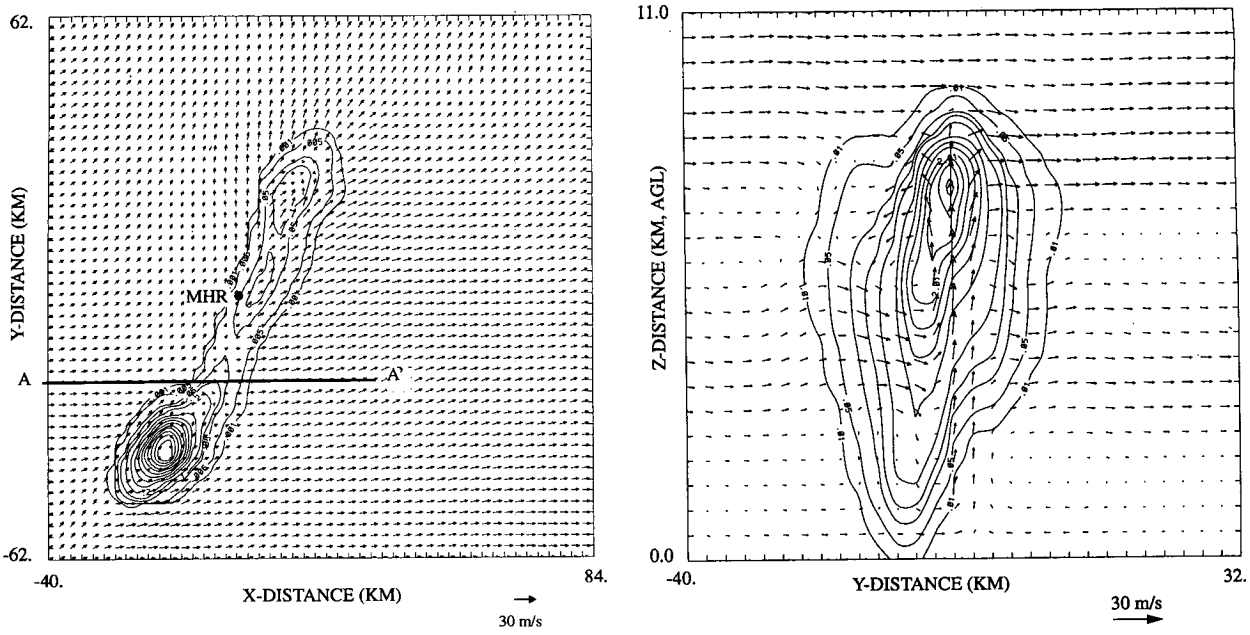

FIG. 6. (a) Horizontal cross section of rainwater and velocity field at 2.5 km AGL, at t = 1400 LT (contour interval, 0.2 g kg^{-1}, with additional contours at 0.001, 0.005, and 0.05 g kg^{-1}). (b) Vertical cross section (along line AA' in 6a) of rainwater and velocity field (contour interval, 0.2 g kg^{-1}, with additional contours at 0.01 and 0.05 g kg^{-1}). MHR denotes the location of Mile High Radar.

ity from Mile High Radar at an elevation of 1.2° at 1630 LT is shown in Fig. 11. A major storm has formed directly over the radar. The convergence line that formed this storm can be seen to the north of the radar.

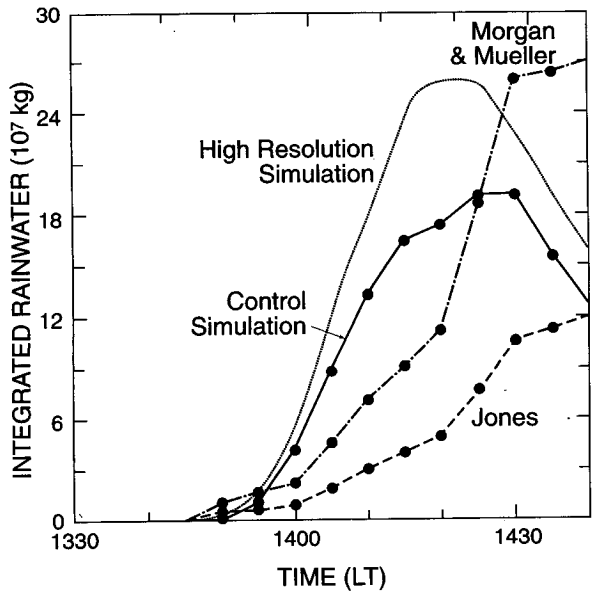

FIG. 7. Domain-integrated rainwater against time for the 21 June case from the control simulation (solid line), from a high-resolution simulation (short-dashed line), from the observed reflectivity using the Morgan and Mueller Z–M relationship (dot–dashed line), and from the observed reflectivity using the Jones Z–M relationship (dashed line).

Unfortunately, due to various hardware problems with MHR on this day, radar data was only collected after 1500 LT. The control experiment was thus initialized at 1500 LT and integrated for 100 m. The CLASS sounding used in the control experiment was modified slightly by mixing out the boundary layer to give a surface temperature of 31.0°C (which was the surface temperature measured at Stapleton minus the 1.0°C temperature bias listed in Table 1). Figure 12a is a horizontal cross section of the rainwater field at 2.5 km AGL at 1630 LT (the same time as shown in Fig. 11). Wind vectors at the surface are overlaid on Fig. 12a. As can be seen, the center of the storm is to the south of the surface convergence line. However, the simulated storm is entirely to the northeast of Mile High Radar, whereas the radar observations show that a portion of the storm formed directly over the radar. A north–south vertical cross section of the rainwater field is plotted in Fig. 12b and shows that significant rain is reaching the ground at this stage. The rainwater integrated over the total domain maximizes at 8.0 $\times 10^7$ kg. The vertical velocity maximizes at 18.5 m s^{-1}.

Again, the total rainwater has been compared with the rainwater estimated from the observed radar reflectivity. Figure 13 shows a time series from 1520 LT of the simulated rainwater amount and that estimated from the observations by the Z–M relationships of Jones (1956) and Morgan and Mueller (1972). As can be seen, the simulated storm begins to develop around 1600 LT, which is about 30 min

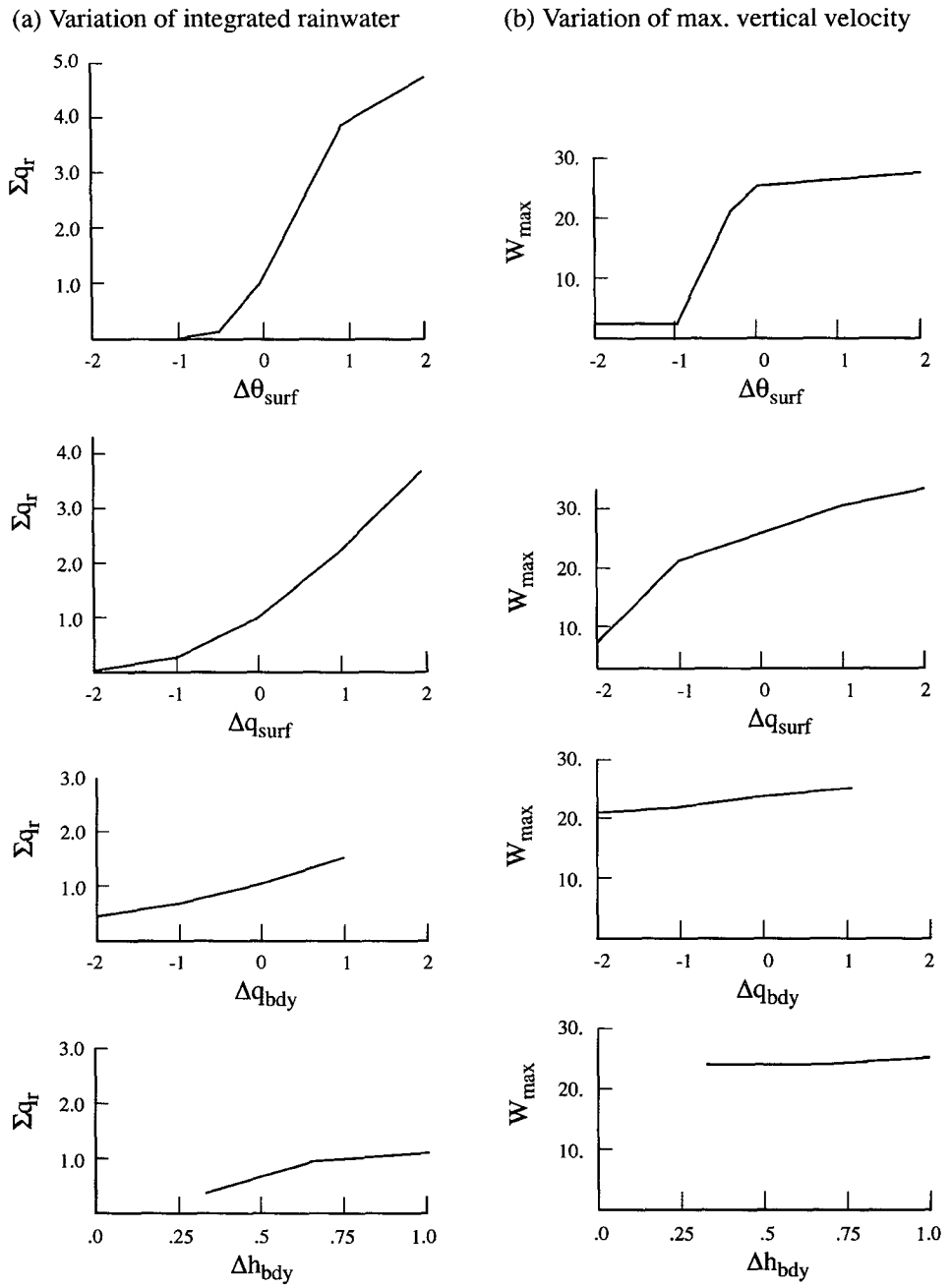

FIG. 8. (a) Variation of integrated rainwater Σq_r against surface temperature dropoff $\Delta\theta_{surf}$, surface moisture dropoff Δq_{surf}, boundary layer moisture dropoff Δq_{bdy} and depth of the moisture Δh_{bdy} for the June 21 case. (b) Same as (a) except for maximum vertical velocity w_{max}.

after the observed storm. This timing error is most likely due to the fact that the model could not be initialized earlier than 1500 LT because of lack of radar data, and thus may have missed some of the convergence that was required to lift air to the level of free convection. Once the simulated storm is initiated, it produces a similar rainwater amount as the Morgan and Mueller estimate.

The sensitivity of Σq_r to the four boundary parameters, $\Delta\theta_{surf}$, Δq_{surf}, Δq_{bdy}, and Δh_{bdy}, is plotted in Fig. 14a. As in the 21 June case, the total rainwater is very sensitive to both $\Delta\theta_{surf}$ and Δq_{surf}. For this case, the convection is more sensitive to Δq_{surf} ($\Sigma q_r = 4.3$ at 2σ) than to $\Delta\theta_{surf}$ ($\Sigma q_r = 3.5$ at 2σ).

The maximum vertical velocity shows a similar behavior to the 21 June case. As $\Delta\theta_{surf}$ is decreased below

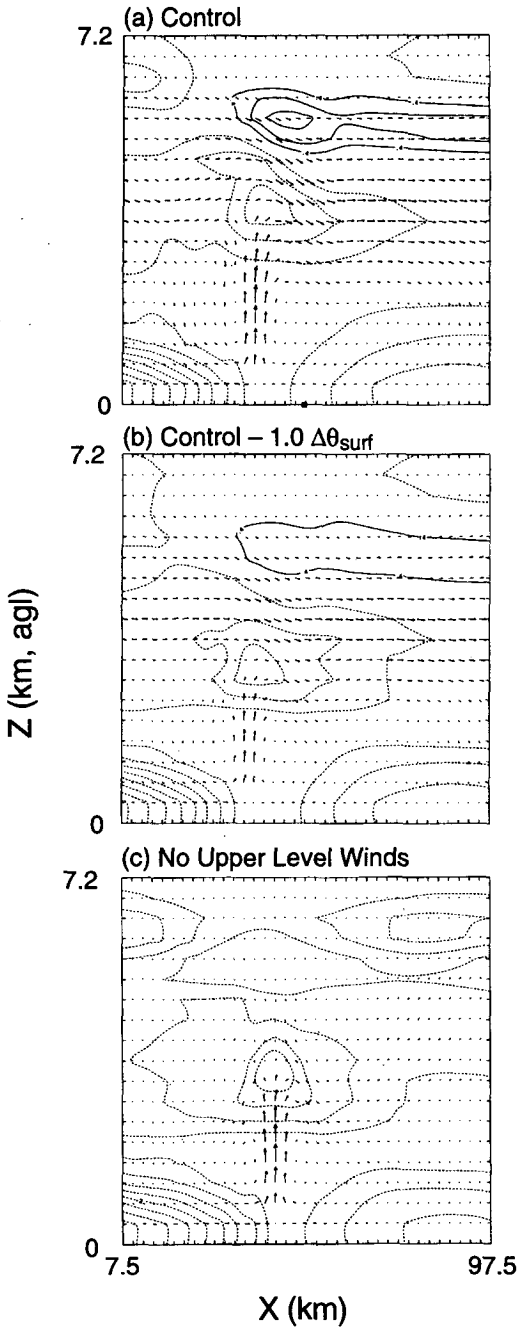

FIG. 9. (a) Vertical cross section of θ' and velocity field through the convergence line in the control simulation. The cross section is along the line AA' in Fig. 6a. Here, θ' represents the deviation from that experiment's base-state sounding. The contour interval is 0.4°C. (b) Same cross section for a simulation with $\Delta\theta_{surf}$ reduced by 1°C. (c) Same simulation as in (b) except with mean wind above the boundary layer set to zero.

the control, w_{max} decreases very rapidly to 4.0 m s^{-1} at -1σ. At values larger than the control, w_{max} increases only slowly. Here, w_{max} is more sensitive to moisture variations, increasing from 2 m s^{-1} at -2σ to 30 m s^{-1} at $+2\sigma$.

Compared to the 21 June case, this case is more sensitive to the parameters, Δq_{bdy} and Δh_{bdy}, that control the shape of the boundary layer moisture profile. As Δq_{bdy} varies from -2σ to $+1\sigma$, Σq_r increases from 50% to 190% of the control. As the depth of the surface moisture decreases to one-third of the total depth of the boundary layer, Σq_r decreases to 20% of the control.

5. Analysis of results

Although there are some differences in the sensitivities between the two case studies, the main results can be summarized as follows:

1) Convection was found to be most sensitive to the temperature and moisture dropoff at the surface, $\Delta\theta_{surf}$ and Δq_{surf}, respectively. As $\Delta\theta_{surf}$ and Δq_{surf} increased from -2σ to $+2\sigma$ the maximum rainwater increased from zero to 4–6 times the control simulation.

2) The maximum vertical velocity was most sensitive to $\Delta\theta_{surf}$ at the convection/no convection boundary. However, for cases with well-developed convection, w_{max} was more sensitive to Δq_{surf}.

3) Convection was least sensitive to the parameters, Δq_{bdy} and Δh_{bdy}, which controlled the shape of moisture profile in the boundary layer.

Some insight into these results can be gained by examining how the positive area (or convective available potential energy, CAPE) and the negative area (or convective inhibition, CIN) changes as the low-level thermodynamics are varied. Since the results have shown

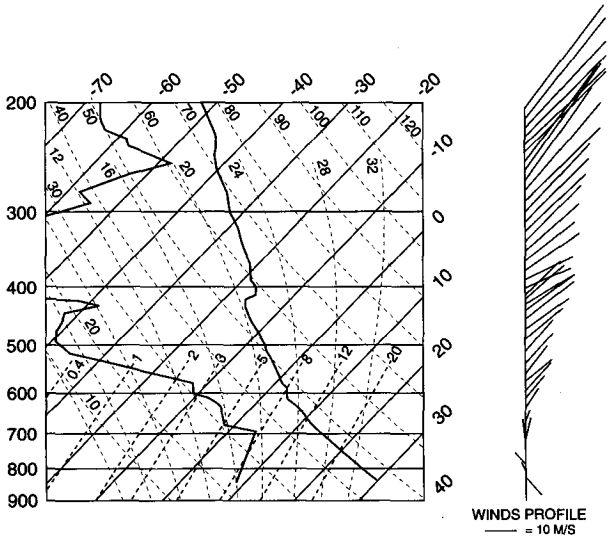

FIG. 10. CLASS sounding taken at Stapleton at 1400 LT 15 July 1993. The sounding used in the control simulation was modified slightly by mixing out the boundary layer to give a surface temperature of 31°C.

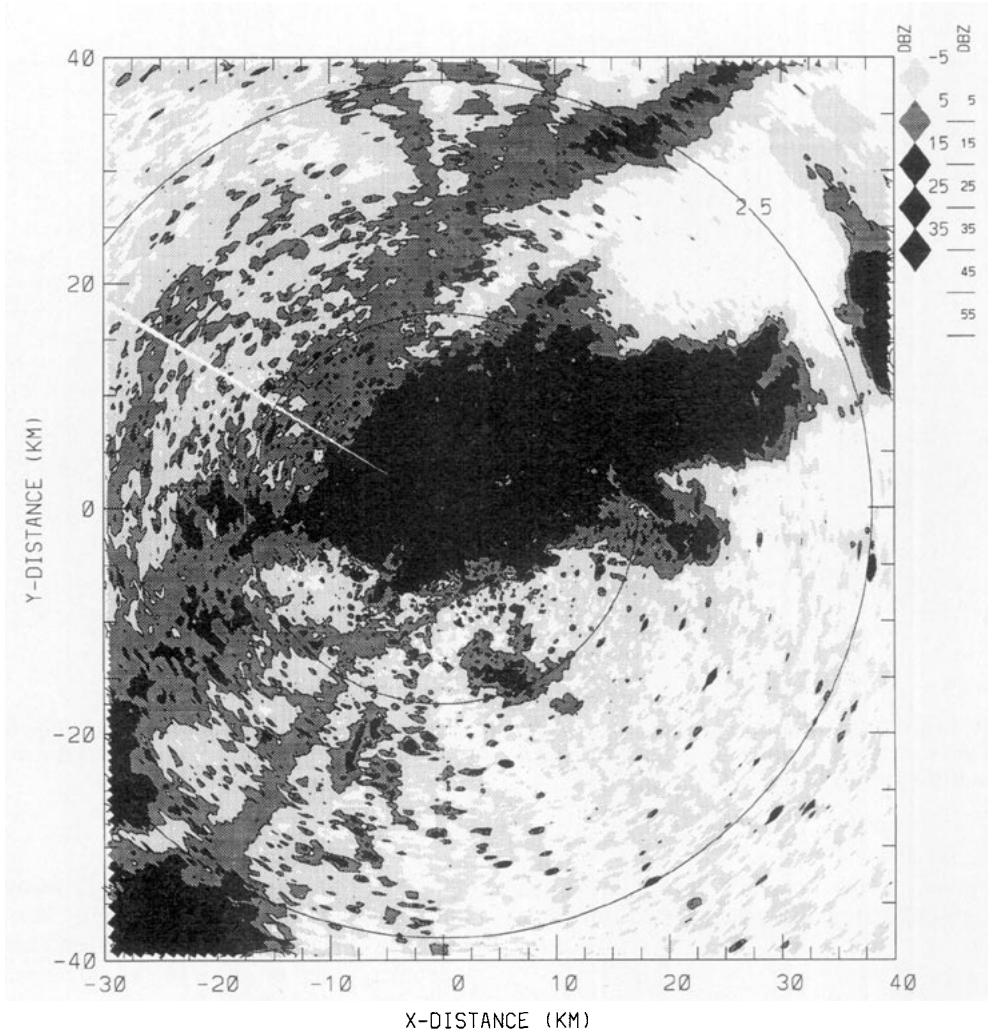

FIG. 11. Reflectivity at an elevation of 1.2° measured by Mile High Radar at 1630 LT 15 July. Convergence line that generated the storm can be seen to the northeast.

that convection is most sensitive to the surface temperature and moisture dropoff, only the sensitivity of CAPE and CIN to $\Delta\theta_{surf}$ and Δq_{surf} will be examined.

a. Analysis of CAPE

As illustrated in Fig. 3, since all of the positive buoyancy occurs under saturated conditions, CAPE depends uniquely on the moist adiabat along which the surface air ascends. Along this moist adiabat, the moist static energy

$$h = gz + c_pT + Lq \tag{5.1}$$

is conserved. Thus, in terms of CAPE, a moisture variation of Δq is equivalent to a temperature variation of $\Delta T = (L/c_p)\Delta q$. Since $L/c_p \approx 2.5$ (mks units), 1 g kg^{-1} is equivalent to 2.5°C. This also means that the typical error in Δq_{surf} (1 g kg^{-1}) has 2.5 times the effect on CAPE compared to the typical error in $\Delta\theta_{surf}$ (1°C).

The fact that moisture and temperature variations are equivalent in terms of CAPE can be seen in the sensitivity plots of w_{max}. Parcel theory, which assumes that the energy released by the buoyancy force is converted entirely into kinetic energy, predicts that

$$\frac{1}{2} w_{max}^2 = \text{CAPE}. \tag{5.2}$$

Figure 15 is a plot of w_{max} against (2 CAPE)$^{1/2}$ for simulations with varying $\Delta\theta_{surf}$ and Δq_{surf}. Only simulations in which convection develops have been plotted. A linear relationship is clearly evident with a correlation coefficient of 0.9. This shows that, in terms of w_{max}, surface moisture variations are equivalent (approximately) to temperature variations with the same moist static energy change.

The slope of the line of best fit, however, is about 0.6, whereas parcel theory predicts a slope of 1. The

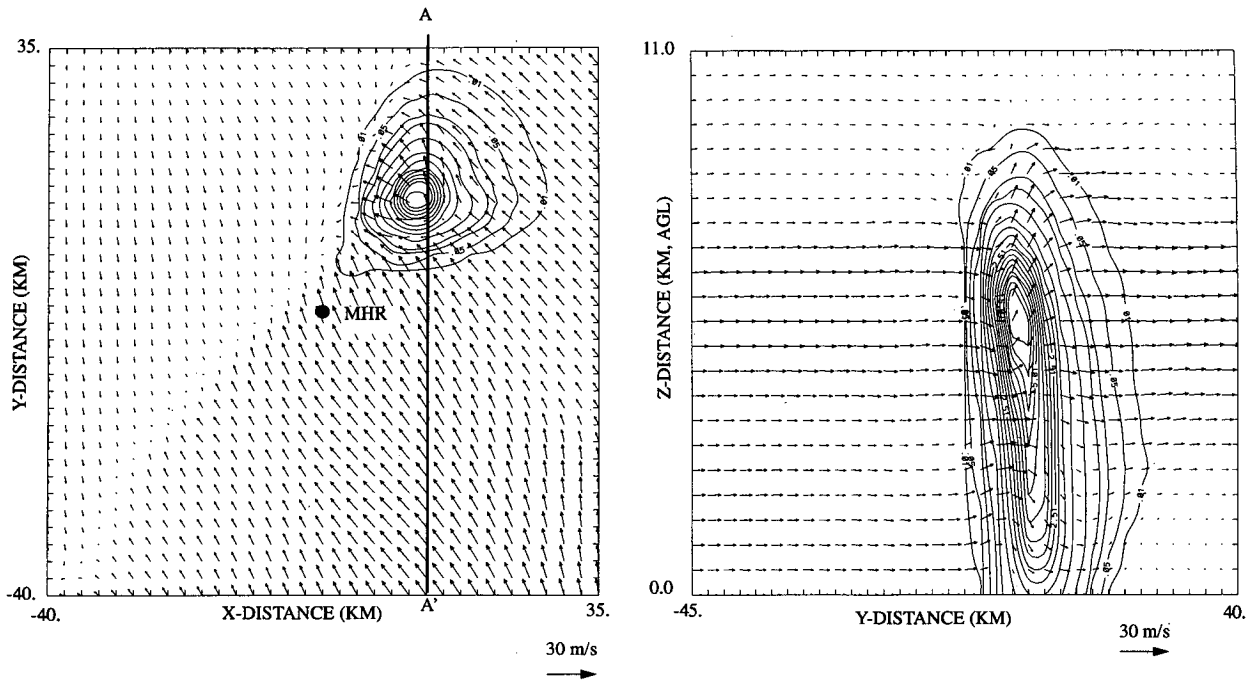

FIG. 12. (a) Horizontal cross section of rainwater field at 2.5 km AGL at 1630 LT (same time as shown in Fig. 11). Contour interval 0.05 g kg^{-1}. Wind vectors at the surface are overlaid. (b) Vertical cross section [along the line AA' in (a)] of the rainwater and velocity field (contour interval 0.05 g kg^{-1}).

reasons that parcel theory generally overpredicts w_{max} are well recognized and include, but are not limited to, the following.

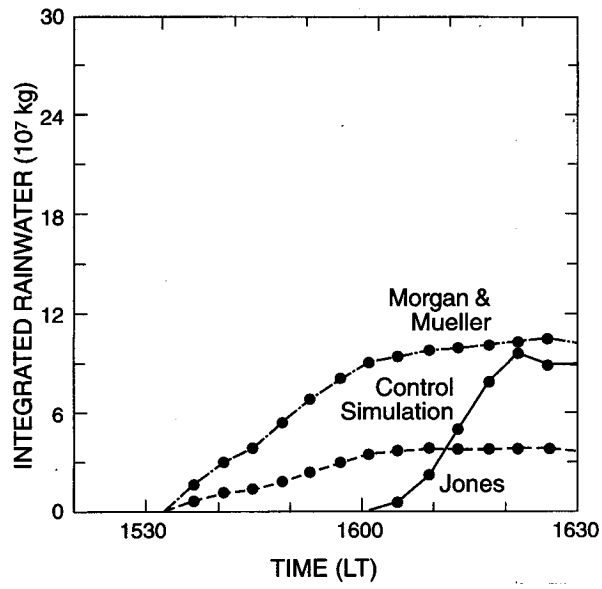

FIG. 13. Domain-integrated rainwater against time for 15 July case from (a) model simulation, (b) observed reflectivity using Jones Z–M relationship, and (c) using Morgan and Mueller Z–M relationship.

1) Waterloading. This reduces the buoyancy of the updraft and hence the potential energy that can be converted into kinetic energy. For a given change in moist static energy, the effect of waterloading will be greater for those cases in which Δq_{surf} is increased compared to cases in which $\Delta\theta_{surf}$ is increased. However, this effect is probably small; in terms of waterloading, a 1 g kg^{-1} increase in Δq_{surf} is equivalent to a 0.3°C decrease in $\Delta\theta_{surf}$ (assuming that all the condensate remains with the air parcel), while in terms of moist static energy, 1 g kg^{-1} of moisture is equivalent to 2.5°C in $\Delta\theta_{surf}$.

2) Diffusion. Mixing of the updraft air with the environment reduces the potential energy that can be converted into kinetic energy. Because of the simple parameterization of mixing that is used in the model, the magnitude of this effect should be similar for cases in which $\Delta\theta_{surf}$ is increased compared to cases in which Δq_{surf} is increased.

3) Shear. The effect of shear on the maximum vertical velocity attained for a given CAPE has been examined by Moncrieff and Green (1972) and Weisman and Klemp (1982) among others. Weisman and Klemp calculated the parameter $S = w_{max}(2\ \text{CAPE})^{-1/2}$ (the ratio of w_{max} to the maximum expected from parcel theory) for a number of simulated storms with varying Richardson number, R [$R \equiv \text{CAPE}(0.5\bar{u}^2)^{-1}$, where $\bar{u}$ represents a difference between the environmental wind speeds at low and midlevels]. They found that for the initial convection, S increased as the Richard-

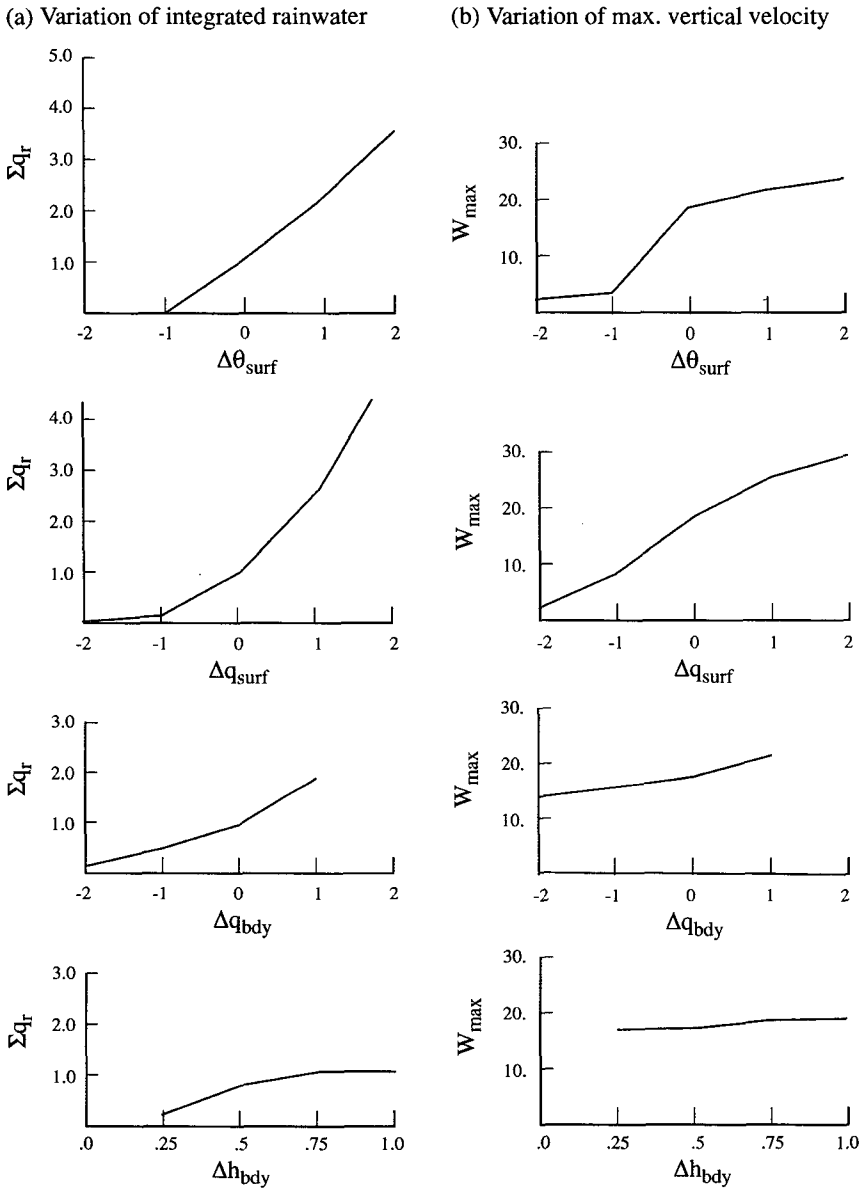

FIG. 14. Same as in Fig. 8 except for the 15 July case.

son number increased [see their Fig. 13a] although above $R \sim 100$ the value of S tended to level off at around 0.6. In the present study in which the shear has been kept fixed, R is directly proportional to CAPE and varies from 20 to 200. Over that parameter regime, S remains relatively constant at a value of approximately 0.6, with no indication of a decrease at smaller values of R. In the Weisman and Klemp (1982) simulations, S varied from 0.40 to 0.58 over this Richardson number range. The reason that the present results differ from the findings of Weisman and Klemp (1982) is not clear, but may be due to the use of different base states or to different initiation mechanisms (convergence line compared to warm bubble).

Despite these limitations with parcel theory, Fig. 15 indicates that some aspects of the convection, particularly the maximum updraft velocity, can be estimated by measuring the CAPE of the environment. This also explains the feature noted previously that for cases in which convection develops, w_{max} is more sensitive to observed moisture variability than to temperature variability, since one standard deviation in moisture variability has 2.5 times the effect on CAPE as one standard deviation in temperature variability.

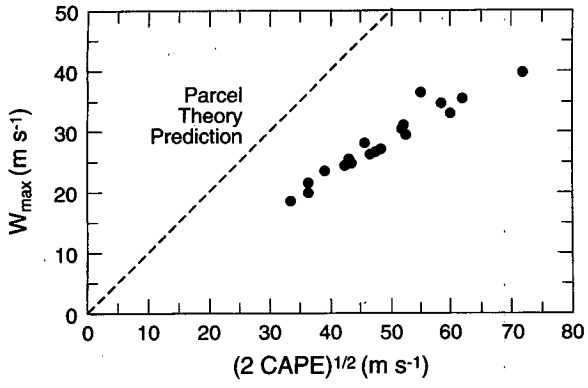

FIG. 15. Maximum vertical velocity w_{max} against (2 CAPE)$^{1/2}$ for all simulations in which convection develops. Shown also is the prediction of parcel theory.

It should be emphasized that the relationship shown in Fig. 15 is only valid for those cases in which convection develops. The magnitude of CAPE does not give any guidance for predicting whether convection will develop or not, which is the main emphasis of this study. As illustrated by Fig. 9, convection initiation depends very sensitively on the magnitude of CIN. For soundings in which the LCL is above the top of the boundary layer, CIN does not depend uniquely on the moist static energy (unlike CAPE). As will be shown, this means that CIN is more sensitive to temperature variations than to moisture variations with the same moist static energy change.

b. Analysis of CIN

The sensitivity of CIN to moisture and temperature variations is illustrated in Fig. 16. The first panel shows a typical summertime sounding plotted on a skew T–log$p$ diagram. The surface temperature and moisture are T_{surf} and q_{surf}, respectively, the top of the boundary layer is at a pressure p_i, the lifting condensation level at p_{lcl}, and the level of free convection at p_{lfc}. On this thermodynamic diagram, CIN is proportional to the stippled area, and is equal to

$$\mathrm{CIN} = \int_{p_{lfc}}^{p_i} R\Delta T \, d\ln(p), \tag{5.3}$$

where ΔT is the temperature difference between the lifted parcel and the environment.

The change in CIN due to moisture variations Δq_{surf} and temperature variations ΔT_{surf} is now considered. Figure 16b illustrates the change in CIN due to an increase in moisture of Δq_{surf}. The decrease in CIN is due solely to the air parcel being warmer in the saturated section of the lifting. The air parcel moves along a moist adiabat that has a moist static energy increased by $L\Delta q_{surf}$. Using the Clausius–Clapeyron equation, it can be shown that the temperature increase along this new moist adiabat is

$$\Delta T_{sat} = \frac{L\Delta q_{surf}}{(c_p + L^2 q_s / R_v T^2)}. \tag{5.4}$$

The change in CIN that this temperature increase causes is approximately

$$\Delta \mathrm{CIN}_{sat} \approx R\overline{\Delta T_{sat}} \ln\left(\frac{p_{lcl}}{p_{lfc}}\right), \tag{5.5}$$

where $\overline{\Delta T_{sat}}$ is the mean value of ΔT_{sat} between p_{lcl} and p_{lfc}. In Eq. (5.5) it has been assumed that the change in CIN due to the difference between the dry-adiabatic lapse rate and the environmental lapse rate is small (in other words, the difference between the areas C' and C'' is small compared to the overall change in CIN).

Figure 16c illustrates the change in CIN due to a temperature increase of ΔT_{surf}. Now the air parcel is not just warmer in the saturated portion of the lifting, but also warmer in the unsaturated section. The temperature increase in the region of unsaturated mixing is

$$\Delta T_{unsat} = \Delta T_{surf}\left(\frac{p}{p_{surf}}\right)^{\kappa}. \tag{5.6}$$

The change in CIN that this temperature increase causes is approximately

$$\Delta \mathrm{CIN}_{unsat} \approx R\Delta T_{surf}\left(\frac{\bar{p}}{p_{surf}}\right)^{\kappa} \ln\left(\frac{p_{lcl}}{p_i}\right), \tag{5.7}$$

where $\bar{p}$ is a mean pressure between p_i and p_{lcl}. Again, it has been assumed that the difference between the two areas D' and D'' is small compared to the overall decrease in CIN.

The change in CIN due to temperature variations compared to the change due to moisture variations can be written as

$$\frac{\Delta \mathrm{CIN(temperature)}}{\Delta \mathrm{CIN(moisture)}} = \frac{\Delta \mathrm{CIN}_{unsat} + \Delta \mathrm{CIN}_{sat}}{\Delta \mathrm{CIN}_{sat}}. \tag{5.8}$$

By setting $c_p \Delta T_{surf} = L_v \Delta q_{surf}$, the change in CIN due to moisture and temperature variations that have equivalent moist static energy difference can be compared. Substituting Eqs. (5.5) and (5.7) into (5.8) and using the expansion $\ln(1 + x) \approx x$ for $|x| \ll 1$, gives

$$\frac{\Delta \mathrm{CIN(temperature)}}{\Delta \mathrm{CIN(moisture)}} = 1 + \left(1 + \frac{L_v^2 q_s}{c_p R_v T^2}\right)\left(\frac{\bar{p}}{p_0}\right)^{\kappa} \frac{(p_i - p_{lcl})}{(p_{lcl} - p_{lfc})} \equiv 1 + A\frac{(p_i - p_{lcl})}{(p_{lcl} - p_{lfc})},$$

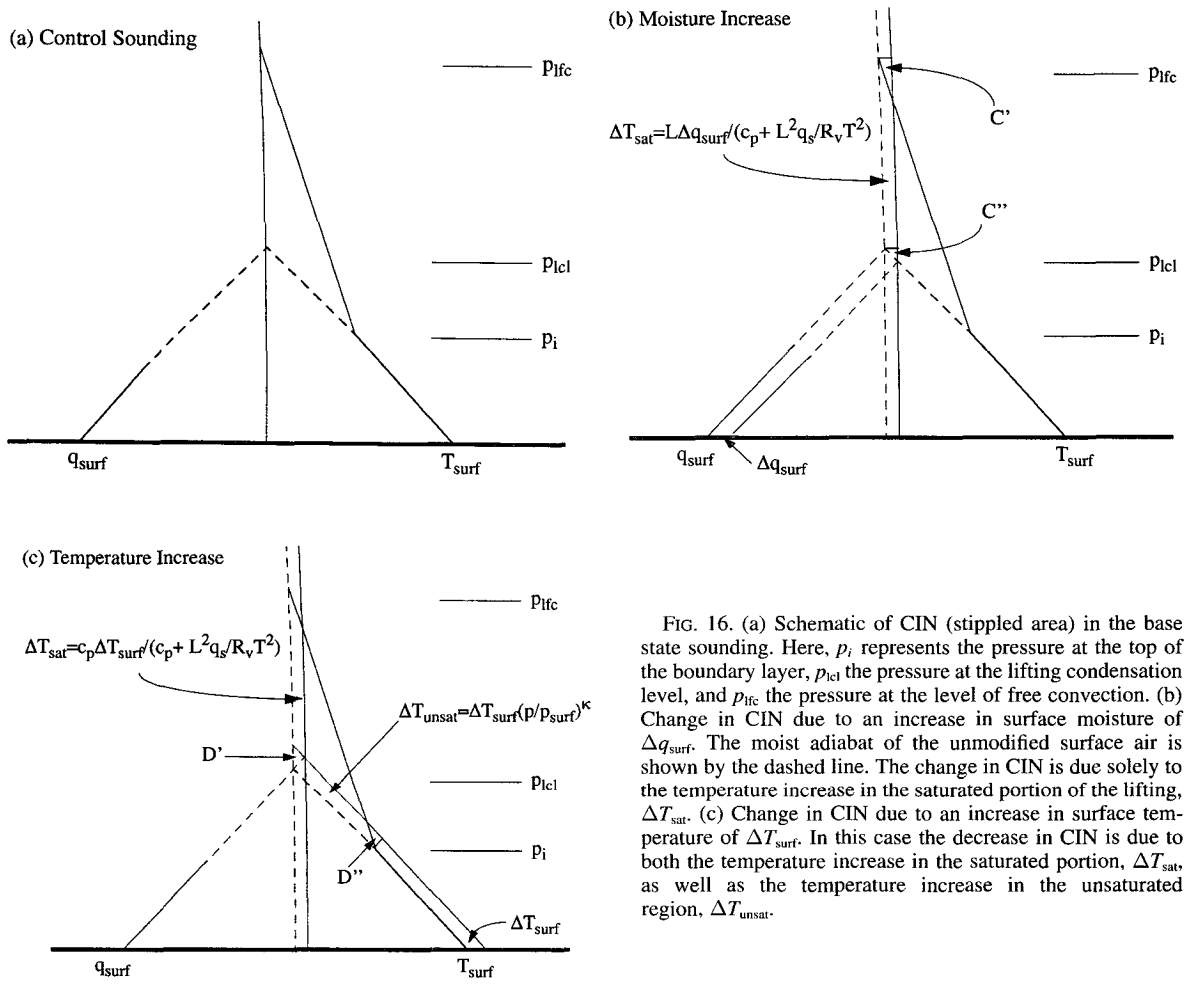

FIG. 16. (a) Schematic of CIN (stippled area) in the base state sounding. Here, p_i represents the pressure at the top of the boundary layer, p_{lcl} the pressure at the lifting condensation level, and p_{lfc} the pressure at the level of free convection. (b) Change in CIN due to an increase in surface moisture of Δq_{surf}. The moist adiabat of the unmodified surface air is shown by the dashed line. The change in CIN is due solely to the temperature increase in the saturated portion of the lifting, ΔT_{sat}. (c) Change in CIN due to an increase in surface temperature of ΔT_{surf}. In this case the decrease in CIN is due to both the temperature increase in the saturated portion, ΔT_{sat}, as well as the temperature increase in the unsaturated region, ΔT_{unsat}.

where

$$A = \left(1 + \frac{L_v^2 q_s}{c_p R_v T^2}\right)\left(\frac{\bar{p}}{p_0}\right)^{\kappa}. \quad (5.9)$$

For typical High Plains summertime conditions, $\bar{p} \sim 600$ mb, $q_s \sim 6$ g kg^{-1} and $T \sim 273$ K, which gives $A \approx 2$. (For warmer climates, A will be higher, since q_s in the numerator increases faster with temperature than T^2 in the denominator. Also, A will be slightly higher for moister climates, as p_{lcl} increases.)

Equation (5.9) indicates that the relative sensitivity of CIN to temperature variations compared to moisture variations depends on the ratio of $(p_i - p_{lcl})$ compared to $(p_{lcl} - p_{lfc})$. In turn, this ratio can be related to the stability of the environment $\partial\theta_{env}/\partial p$ compared to the moist potential temperature lapse rate $\partial\theta_{sat}/\partial p$. Since the change in potential temperature of the environment between p_i and p_{lfc} must equal the change in potential temperature along the moist adiabat between p_{lcl} and p_{lfc} (see Fig. 16a), it follows that

$$\frac{\partial\theta_{env}}{\partial p}(p_i - p_{lfc}) = \frac{\partial\theta_{sat}}{\partial p}(p_{lcl} - p_{lfc}). \quad (5.10)$$

Therefore,

$$\frac{\Delta\text{CIN(temperature)}}{\Delta\text{CIN(moisture)}} = 1 + A\left[\left(\frac{\partial\theta_{sat}}{\partial p}\right)\left(\frac{\partial\theta_{env}}{\partial p}\right)^{-1} - 1\right]. \quad (5.11)$$

Thus, the relative sensitivity of CIN to temperature and moisture variations depends on the ratio of the environmental stratification to the moist potential temperature lapse rate. When $\partial\theta_{env}/\partial p = \partial\theta_{sat}/\partial p$ then $\Delta\text{CIN(temperature)}/\Delta\text{CIN(moisture)} = 1$ since in this limit the LCL is at the top of the boundary layer and all of the lifting occurs under saturated conditions.

For the soundings used in this study, $\partial\theta_{sat}/\partial p \sim 3\partial\theta_{env}/\partial p$. Hence, for the same moist static energy, CIN for these soundings is 5–6 times more sensitive to temperature variations than to moisture variations. To express this in terms of typical observational error, it is first noted that one standard deviation in moisture error (1 g kg^{-1}) has 2.5 times the effect on moist static energy as one standard deviation

in temperature error (1°C). Hence, in terms of observational error, CIN is still more sensitive to temperature variations than to moisture variations (in the cases studied). Finally, this explains the fact that at the convection/no convection boundary, the maximum vertical velocity is more sensitive to temperature errors than to moisture errors (see Figs. 8b and 14b).

As already discussed, some of the conclusions about the relative sensitivity of CIN will depend on the particular form of the thermodynamic profile. Usually, the stratification above the boundary layer is stronger than in the cases studied herein which, from Eq. (5.11), will decrease the sensitivity of CIN to temperature variations compared to moisture variations. However, as previously discussed, in warmer, moister environments, the parameter A is larger, which has the opposite effect of increasing the sensitivity to temperature compared to moisture.

6. Discussion

The results presented in the previous sections indicate that convection initiation is very sensitive to variations in boundary layer thermodynamics that are difficult to detect with the present observing system. A similar result, at least for temperature, was reported by Brooks et al. (1993), who found that the structure of a simulated storm changed significantly when the low-level temperature was altered by 1.0°C. In turn, these results suggest that convection initiation has limited predictability at least for numerical models initialized with data from the present observing system. Three approaches that could lead to improved predictability are now discussed.

1) More accurate initial conditions. The most obvious method to increase the predictability of the numerical forecasts is to improve the accuracy of the initial conditions. Unfortunately, with the present observing system of twice-daily soundings and surface measurements, there is not a large potential for increased accuracy. Some improvements could be gained if the sources of the error in the parameters $\Delta\theta_{\text{surf}}$, Δq_{surf}, Δq_{bdy}, and Δh_{bdy}, were better understood and could be more accurately parameterized. The analysis in the previous section has shown that CIN is most sensitive to the surface temperature dropoff, hence of the parameters examined in this study, the greatest improvement in convective initiation predictability, should arise from improvements in the parameterization of $\Delta\theta_{\text{surf}}$.

New technologies for observing the low-level thermodynamic fields should also result in improved initial conditions. Radio acoustic sounding systems (RASS) can give high resolution ($\leq$300 m) profiles of virtual potential temperature throughout the convective boundary layer every 30 min. Comparisons of RASS data from Denver with over 50 radiosonde ascents showed rms differences of 1°C (May et al. 1989). Since this is similar to the accuracy of surface mesonet temperatures, it could be argued that these observations will not improve the problem of thunderstorm predictability. However, since RASS measures a profile of boundary layer temperature, it will remove the necessity of making assumptions about that profile.

Measurements of boundary layer moisture on a continuous basis are somewhat more problematic. The CASH program (commercial aviation sensing of humidity, Fleming and Hills 1993) will provide some low-level measurements, especially around airports. GPS (Global Positioning System, Ware et al. 1996) observations can provide very accurate measurements of column-integrated water. However, before these measurements can be used, it is necessary to make a number of assumptions about the distribution of moisture through the entire depth of the atmosphere. Finally, Raman lidar offers the potential of high-resolution profiling of low-level moisture; however, currently its use is limited to night-time operations (Goldsmith et al. 1994).

2) Ensemble forecasting. One method of improving the predictability of atmospheric flows is to perform a number of simulations each starting with slightly different initial conditions. As long as the different initial conditions span the domain of expected error in the initial fields, the ensemble mean should provide a better forecast than most individual forecasts. Ensemble forecasting has recently been implemented at ECMWF and NMC (Tracton and Kalnay 1993) for long-range forecasting. A considerable amount of research is currently being performed on the viability of ensemble forecasting on the short range (0–48 h) (see Brooks et al. 1995 for a discussion). The results presented in this study concerning the magnitude of error growth in convective flows suggests that ensemble forecasting would also be beneficial for the thunderstorm initiation problem.

3) Using analyzed and predicted fields for guidance. Although the results presented above have suggested that *explicit* numerical forecasts of thunderstorm initiation have limited predictability, some of the model fields may provide guidance to the operational forecaster. Several observational studies have shown that the surface moisture convergence field is a useful predictor for storm initiation (see, e.g., Byers and Braham 1949; Watson and Blanchard 1984; Ulanski and Garstang 1978; Fankhauser 1988). It should be noted that the reason that surface moisture convergence acts as a good predictor for storm initiation is that it generally correlates well with regions where unstable air is being lifted to the LFC. However, using surface convergence alone can sometimes lead to misleading results.

To illustrate this point, the surface moisture convergence is plotted from the 21 June, control simulation (Fig. 17a) and from the simulation with the $\Delta\theta_{\text{surf}}$ reduced by one standard deviation (1°C), Fig. 17b. The fields are plotted at 1345 LT, which is just before con-

vection develops in the control simulation. The maximum moisture convergence in the control simulation is 1.3×10^{-6} s^{-1}. In the $\Delta\theta_{surf} = -\sigma$ simulation it is 1.1×10^{-6} s^{-1}, which is a reduction of only 15%.[2] However, as already noted, no convection develops in this second simulation.

The reason that no convection develops in the second simulation, despite the fact that there is significant surface moisture convergence, is that the unstable air at the surface is not being lifted to the LFC because of the increased negative area at the top of the boundary layer. In this latter simulation there is sufficient divergence below the LFC to offset the convergence at lower levels. This suggests that a field that takes into account the integrated convergence/divergence throughout the depth of the boundary layer would be more useful for indicating the potential for convection initiation.

A candidate for this field is the vertical moisture flux at the top of the boundary layer. In Fig. 18, this field is plotted at 1345 LT in the control simulation and in the $\Delta\theta_{surf} = -\sigma$ simulation. In the control simulation the maximum flux is 75 g kg^{-1} m s^{-1}, while in the $\Delta\theta_{surf} = -\sigma$ simulation, the maximum is 15 g kg^{-1} m s^{-1}, which is a reduction of 80%. Hence, the change in vertical moisture flux at the top of the boundary layer more accurately reflects the potential for convective initiation than does the surface moisture convergence. Of course, it could be argued that even though the vertical moisture flux is a more discriminating field, it is more difficult to analyze and predict accurately due in part to the observational errors outlined in this paper. Nevertheless, the accuracy of fields in, and above, the boundary layer such as the vertical moisture flux should improve as more remote sensing platforms are deployed and as data assimilation techniques continue to improve.

7. Conclusions

This paper has examined the sensitivity of thunderstorm initiation to a number of boundary layer thermodynamics parameters. These parameters include the surface temperature dropoff, the surface moisture dropoff, the boundary layer moisture dropoff, and the depth of the moisture. The typical variability in the first three parameters was examined using data from CINDE and the RAPS project.

"Forward" sensitivity experiments were then performed on two convection initiation cases from the RAPS93 project. The general findings from these experiments are

1) convection was found to be most sensitive to the surface temperature dropoff, $\Delta\theta_{surf}$, and the surface moisture dropoff, Δq_{surf}.

2) The maximum vertical velocity was most sensitive to $\Delta\theta_{surf}$ at the convection/no convection boundary. It was shown that the convective inhibition (CIN) is more sensitive to temperature variations than to moisture variations in terms of equivalent moist static energy and, for the cases studied herein, in terms of typical observational error.

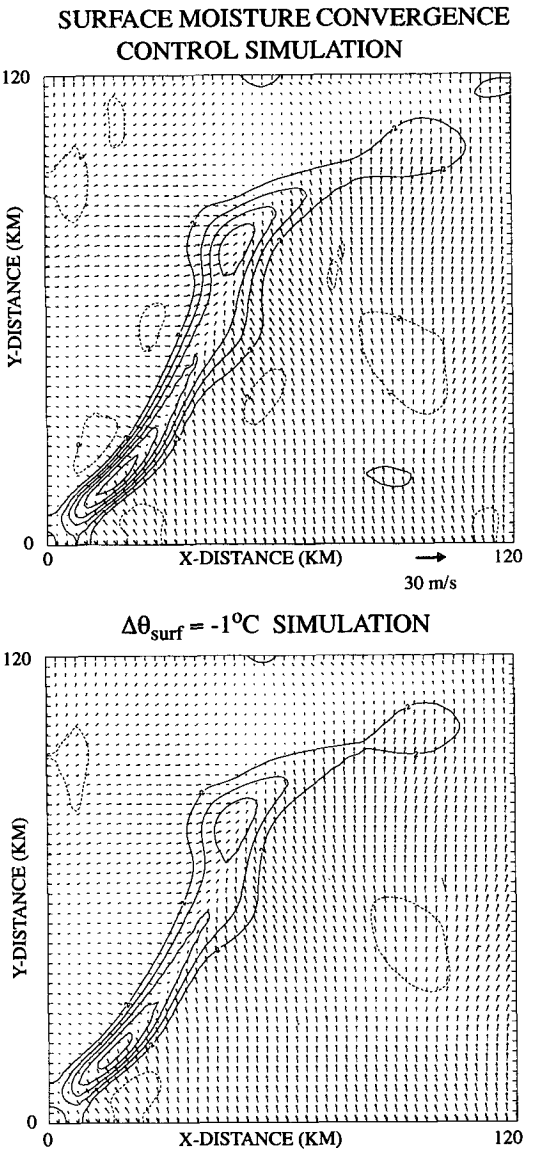

FIG. 17. Surface moisture convergence just prior to convection initiation (1345 LT) from the (a) control simulation and (b) simulation with ΔT_{surf} reduced by 1.0°C. Contour interval is 2×10^{-7} s^{-1}.

[2] Since the initial flow field is the same in the two simulations, this result indicates that the surface moisture convergence develops slightly more slowly in the $\Delta\theta_{surf} = -\sigma$ simulation due to the shallower boundary layer (which is the only external parameter that varies between the two simulations). This is presumably due to a feedback between the convergence line and the negative buoyancy generated above; however, the exact nature of that feedback is unclear at the moment.

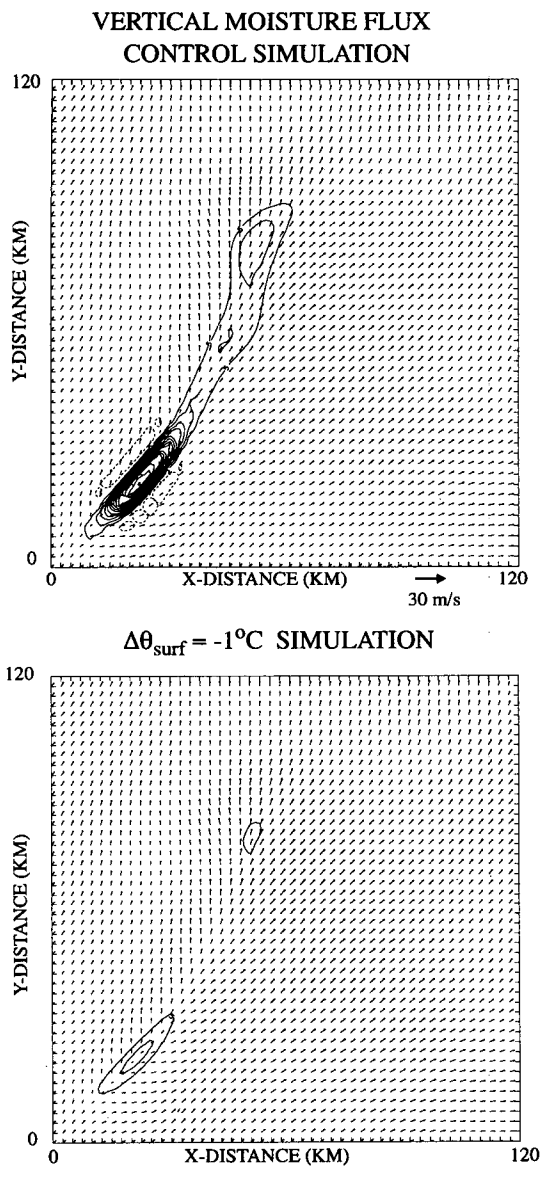

FIG. 18. Vertical moisture flux at the top of the boundary layer (z = 2.0 km, AGL) at the same time shown in Fig. 17 in (a) the control simulation and (b) simulation with ΔT_{surf} reduced by 1.0°C. Contour interval is 5 g kg^{-1} m s^{-1}.

3) For cases with well-developed convection, the maximum vertical velocity w_{max} was more sensitive in terms of observational error to Δq_{surf} than to $\Delta\theta_{surf}$. It is shown that w_{max} correlates well with the environment's CAPE, which in turn is directly proportional to the moist static energy of the low-level air. In terms of moist static energy, the typical error in Δq_{surf} (1 g kg^{-1}) is 2.5 times greater than the typical error in $\Delta\theta_{surf}$ (1°C).

4) Convection was least sensitive to the parameters Δq_{bdy} and Δh_{bdy}, which controlled the shape of the moisture profile in the boundary layer.

It should be noted that in both cases studied herein, the convection was forced primarily by boundary layer processes. Although the convergence in these cases was large, the forcing has been confined primarily to the boundary layer. It is quite possible that moist convection that develops from deeper forcing, for example in larger-scale synoptic systems, is less sensitive to the parameters described herein.

As mentioned in the introduction, convection initiation is a vast problem, which this study has only begun to explore. It is hoped that the present work has indicated some areas for further research.

Acknowledgments. This research is sponsored by the National Science Foundation through an interagency agreement in response to requirements and funding by the Federal Aviation Administration's Aviation Weather Development Program. Reviews of an early version of this paper by Juanzhen Sun, Jimy Dudhia, Fred Carr, and Alan Shapiro are gratefully acknowledged.

REFERENCES

Battan, L. J., 1973: *Radar Observations of the Atmosphere.* University of Chicago Press, 324 pp.

Benjamin, S. G., 1989: An isentropic meso-alpha scale analysis system and its sensitivity to aircraft and surface observations. *Mon. Wea. Rev.*, **117,** 1586–1603.

Brewster, K., F. Carr, N. Lin, J. Straka, and J. Krause, 1994: A local analysis system for initializing real-time convective-scale models. Preprints, *Tenth Conference on Numerical Weather Prediction.* Portland, OR, Amer. Meteor. Soc., 596–598.

Brooks, H. E., C. A. Doswell III, and L. J. Wicker, 1993: STORM-TIPE: A forecasting experiment using a three-dimensional cloud model. *Wea. Forecasting,* **8,** 352–362.

——, M. S. Tracton, D. J. Stensrud, G. DiMego, and Z. Toth, 1995: Short-range ensemble forecasting: Report from a workshop, 25–27 July 1994. *Bull. Amer. Meteor. Soc.,* **76,** 1617–1624.

Byers, H. R., and R. R. Braham, 1949: *The Thunderstorm.* U.S. Government Printing Office, 287 pp.

Clark, T. L., 1977: A small scale numerical model using a terrain following coordinate transformation. *J. Comput. Phys.,* **24,** 186–215.

——, and R. D. Farley, 1984: Severe downslope windstorm calculations in two and three spatial dimensions using anelastic interactive grid nesting: A possible mechanism for gustiness. *J. Atmos. Sci.,* **41,** 329–350.

Cole, R., F. W. Wilson Jr., J. McGinley, and S. Albers, 1993: ITWS Gridded Analysis. Preprints, *Fifth International Conference Aviation Weather Systems,* Vienna, VA, Amer. Meteor. Soc., 56–60.

Crook, N. A., 1994: Numerical simulations initialized with radar-derived winds. Part I: Simulated data experiments. *Mon. Wea. Rev.,* **122,** 1189–1203.

——, and J. D. Tuttle, 1994: Numerical simulations initialized with radar-derived winds. Part II: Forecasts of three gust-front cases. *Mon. Wea. Rev.,* **122,** 1204–1217.

Droegemeier, K. K., and R. B. Wilhelmson, 1985a: Three-dimensional numerical modeling of convection produced by interacting outflows. Part I: Control simulation and low-level moisture variations. *J. Atmos. Sci.,* **42,** 2381–2403.

——, and ——, 1985b: Three-dimensional numerical modeling of convection produced by interacting outflows. Part II: Variations in vertical wind shear. *J. Atmos. Sci.,* **42,** 2404–2414.

Errico, R. M., and T. Vukicevic, 1992: Sensitivity analysis using an adjoint of the PSU–NCAR mesoscale model. *Mon. Wea. Rev.*, **120,** 1644–1660.

Fankhauser, J. C., 1988: Estimates of thunderstorm precipitation efficiency from field measurements in CCOPE. *Mon. Wea. Rev.*, **116,** 663–684.

Fleming, R. J., and A. J. Hills, 1993: Humidity profiles via commercial aircraft. *Proc. Eighth Symp. on Meteorological Observations and Instrumentation,* Anaheim, CA, Amer. Meteor. Soc., J125–J129.

Gal-Chen, T., 1978: A method for the initialization of the anelastic equations: Implications for matching models with observations. *Mon. Wea. Rev.*, **106,** 587–606.

Goldsmith, J. E. M., S. E. Bisson, R. A. Ferrare, K. D. Evans, D. N. Whiteman, and S. H. Melfi, 1994: Raman lidar profiling of atmospheric measurements with two collocated systems. *Bull. Amer. Meteor. Soc.*, **75,** 975–982.

Jones, D. M. A., 1956: Rainfall drop-size distribution and radar reflectivity. Research Rep. 6, Urbana: Meteorological Laboratory, Illinois State Water Survey.

Kessler, E., 1969: *On the Distribution and Continuity of Water Substance in Atmospheric Circulations. Meteor. Monogr.,* No. 32, Amer. Meteor. Soc., 84 pp.

Lee, B. D., R. D. Farley, and M. R. Hjelmfelt, 1991: A numerical case study of convection initiation along colliding convergence boundaries in northeast Colorado. *J. Atmos. Sci.*, **48,** 2350–2366.

Lilly, D. K., 1962: On the numerical simulation of buoyant convection. *Tellus,* **14,** 148–172.

Mahrt, L., 1976: Mixed layer moisture structure. *Mon. Wea. Rev.*, **104,** 1403–1407.

May, P. T., K. P. Moran, and R. G. Strauch, 1989: The accuracy of RASS temperature measurements. *J. Appl. Meteor.*, **28,** 1329–1335.

McGinley, J. A., 1989: The local analysis and prediction system. *Proc. 12th Conference on Weather Analysis and Forecasting,* Monterey, CA, Amer. Meteor. Soc., 15–20.

Moncrieff, M. W., and J. S. A. Green, 1972: The propagation and transfer properties of steady convective overturning in shear. *Quart. J. Roy. Meteor. Soc.*, **98,** 336–352.

Morgan, G. M., and E. A. Mueller, 1972: The total liquid water mass of large convective storms. *Proc. 15th Radar Meteorology Conference,* Champaign-Urbana, IL, Amer. Meteor. Soc., 39–40.

Mueller, C. K., J. W. Wilson, and N. A. Crook, 1993: The utility of sounding and mesonet data to nowcast thunderstorm initiation. *Wea. Forecasting,* **8,** 132–146.

Neilley, P. P., N. A. Crook, E. A. Brandes, M. Dixon, C. Kessinger, C. Mueller, R. Roberts, J. Tuttle, and J. W. Wilson, 1993: The real-time analysis and prediction of storms program. *Proc. Fifth International Conference on Aviation Weather Systems,* Vienna, VA, Amer. Meteor. Soc., 62–64.

Smagorinsky, J., 1963: General circulation experiments with the primitive equations. I: The basic experiment. *Mon. Wea. Rev.*, **91,** 99–164.

Sun, J., N. A. Crook, and J. Verlinde, 1994: Dynamical and microphysical retrieval from Doppler radar observations using a cloud model and its adjoint. *Proc. 10th Conference on Numerical Weather Prediction,* Portland, OR, Amer. Meteor. Soc., 466–468.

Tracton, M. S., and E. Kalnay, 1993: Operational ensemble prediction at the National Meteorological Center: Practical aspects. *Wea. Forecasting,* **8,** 379–398.

Tuttle, J. D., and G. B. Foote, 1990: Determination of the boundary layer airflow from a single Doppler radar. *J. Atmos. Oceanic Technol.*, **7,** 218–232.

Urlanski, S. L., and M. Garstang, 1978: The role of surface divergence and vorticity in the life cycle of convective rainfall. Part I: Observations and analysis. *J. Atmos. Sci.*, **35,** 1047–1062.

Ware, R., and Coauthors, 1996: GPS sounding of the atmosphere from low earth orbit: Preliminary results. *Bull. Amer. Meteor. Soc.*, **77,** 19–40.

Watson, A. I., and D. O. Blanchard, 1984: The relationship between the total area divergence and convective precipitation in south Florida. *Mon. Wea. Rev.*, **112,** 673–685.

Weisman, M. L., and J. B. Klemp, 1982: The dependence of numerically simulated convective storms on vertical wind shear and buoyancy. *Mon. Wea. Rev.*, **110,** 504–520.